Astronomy & Astrophysics manuscript no. output
September 6, 2022

Letter to the Editor

Detection of Barium in the atmospheres of ultra-hot gas giants WASP-76b & WASP-121b

And new detections of Co and Sr+ on WASP-121b

T. Azevedo Silva[1,2⋆], O. D. S. Demangeon[1,2,⋆⋆], N. C. Santos[1,2], R. Allart[3,4], F. Borsa[5], E. Cristo[1,2], E. Esparza-Borges[6,7], J. V. Seidel[8], E. Palle[9], S. G. Sousa[1], H. M. Tabernero[10], M. R. Zapatero Osorio[10], S. Cristiani[11], F. Pepe[4], R. Rebolo[6,7], V. Adibekyan[1,2], Y. Alibert[12], S. C. C. Barros[1,2], V. Bourrier[4], P. Di Marcantonio[11], V. D'Odorico[11,13,14], D. Ehrenreich[4,15], P. Figueira[4,1], J. I. González Hernández[6,16], C. J. A. P. Martins[1,17], A. Mehner[8], G. Micela[18], P. Molaro[11,19], D. Mounzer[4], N. J. Nunes[20,21], A. Sozzetti[22], A. Suárez Mascareño[6,7], and S. Udry[4]

[1] Instituto de Astrofísica e Ciências do Espaço, Universidade do Porto, CAUP, Rua das Estrelas, 4150-762 Porto, Portugal
[2] Departamento de Física e Astronomia, Faculdade de Ciências, Universidade do Porto, Rua do Campo Alegre, 4169-007 Porto, Portugal.
[3] Department of Physics, and Institute for Research on Exoplanets, Université de Montréal, Montréal, H3T 1J4, Canada.
[4] Observatoire astronomique de l'Université de Genève, Chemin Pegasi 51, 1290 Versoix, Switzerland.
[5] INAF – Osservatorio Astronomico di Brera, Via Bianchi 46, 23807 Merate, Italy.
[6] Instituto de Astrofísica de Canarias (IAC), 38205 La Laguna, Tenerife, Spain.
[7] Departamento de Astrofísica, Universidad de La Laguna, E-38206, La Laguna, Tenerife, Spain.
[8] European Southern Observatory, Alonso de Cordova 3107, Vitacura, Region Metropolitana, Chile.
[9] Instituto de Astrofísica de Canarias, C. Vía Láctea, s/n, E-38205, Spain.
[10] Centro de Astrobiología (CSIC-INTA), Crta. Ajalvir km 4, E-28850 Torrejón de Ardoz, Madrid, Spain.
[11] INAF – Osservatorio Astronomico di Trieste, via G. B. Tiepolo 11, I-34143, Trieste, Italy.
[12] Physikalisches Institut, University of Bern, Sidlerstrasse 5, 3012 Bern, Switzerland.
[13] Scuola Normale Superiore, Piazza dei Cavalieri 7, I-56126 Pisa, Italy.
[14] Institute for Fundamental Physics of the Universe, Via Beirut 2, I-34151 Miramare, Trieste, Italy.
[15] Centre Vie dans l'Univers, Faculté des sciences de l'Université de Genève, Quai Ernest-Ansermet 30, 1205 Geneva, Switzerland.
[16] Universidad de La Laguna (ULL), Departamento de Astrofísica, 38206 La Laguna, Tenerife, Spain.
[17] Centro de Astrofísica da Universidade do Porto, Rua das Estrelas, 4150-762 Porto, Portugal.
[18] INAF – Osservatorio Astronomico di Palermo, Piazza del Parlamento 1, Palermo, Italy.
[19] Institute for Fundamental Physics of the Universe, Via Beirut 2, I-34151 Miramare, Trieste, Italy.
[20] Instituto de Astrofísica e Ciências do Espaço, Faculdade de Ciências da Universidade de Lisboa
[21] Departamento de Física, Faculdade de Ciências da Universidade de Lisboa, Campo Grande, Edificio C8, P-1749-016, Lisboa, Portugal.
[22] INAF - Osservatorio Astrofisico di Torino, Via Osservatorio 20, I-10025 Pino Torinese (TO), Italy.

Received September 15, 1996; accepted March 16, 1997

ABSTRACT

Context. High-resolution spectroscopy studies of ultra-hot Jupiters have been key in our understanding of exoplanet atmospheres. Observing into the atmospheres of these giant planets allows for direct constraints on their atmospheric compositions and dynamics while laying the groundwork for new research regarding their formation and evolution environments.
Aims. Two of the most well-studied ultra-hot Jupiters are WASP-76b and WASP-121b, with multiple detected chemical species and strong signatures of their atmospheric dynamics. We take a new look at these two exceptional ultra-hot Jupiters by re-analyzing the transit observations taken with ESPRESSO at the VLT and attempt to detect the presence of additional species.
Methods. To extract the planetary spectra of both targets, we correct for the telluric absorption and remove the stellar spectrum contributions. We then exploit new synthetic templates specifically designed for ultra-hot Jupiters in combination with the cross-correlation technique to unveil species undetected by previous analyses.
Results. We add a novel detection of Ba+ to the known atmospheric compositions of WASP-76b and WASP-121b, the heaviest species detected to date in any exoplanetary atmosphere, with additional new detections of Co and Sr+ and tentatively Ti+ for WASP-121b. We also confirm the presence of Ca+, Cr, Fe, H, Li, Mg, Mn, Na and V on both WASP-76b and WASP-121b, with the addition of Ca, Fe+ and Ni for the latter. Finally, we also confirm the clear asymmetric absorption feature of Ca+ on WASP-121b, with an excess absorption at the bluer wavelengths and an effective planet radius beyond the Roche-Lobe, hinting that the signal may arise from planetary atmospheric escape.

Key words. Planets and satellites: atmospheres – Planets and satellites:composition – Planets and satellites:gaseous planets – Techniques: spectroscopic – Planets and satellites: individual: WASP-76b, WASP-121b

1. Introduction

Ultra-hot Jupiters are currently the most accessible laboratories for the study of exoplanet atmospheres. Their size and large atmospheric scale heights, combined with the proximity to the host stars, make them appealing targets for the study of light transmitted through planetary atmospheres. With the recent developments on instruments for high-resolution spectroscopy (e.g. ESPRESSO, Pepe et al. 2010, 2021), the enhanced ability to retrieve high-resolution planetary spectra from the transit observations of ultra-hot Jupiters provided unique glimpses into the atmosphere of these extreme worlds. From the detection of several chemical species (e.g. Casasayas-Barris et al. 2019; Tabernero et al. 2021), to evaporating atmospheres (e.g. Yan & Henning 2018) and the study of winds (e.g. Ehrenreich et al. 2020; Seidel et al. 2021), resolving line features over short exposures has proven to be key to unravel these distant alien atmospheres.

Two of the best examples can be found with WASP-76b and WASP-121b (West et al. 2016; Delrez et al. 2016). Both planets are inflated ultra-hot Jupiters on orbits with periods under two days and equilibrium temperatures close to 2500 K (for more information see Appendix A.1). Observed with ESPRESSO, with one of the observing nights using the four VLT UT's, these targets are currently benchmarks in the study of atmospheric composition and dynamics (Seidel et al. 2019; Ehrenreich et al. 2020; Tabernero et al. 2021; Fortney et al. 2021; Sánchez-López et al. 2022). Transmission spectroscopy studies report the detection of species from H[1], Li, Na, Mg, K, Ca+, V, Cr, Mn, Fe, Co[1], Ni and Sr+ for WASP-76b (Tabernero et al. 2021; Kesseli et al. 2022) and H, Li, Na, Mg, K, Ca, Ca+, Sc+, V, Cr, Mn[1], Fe, Fe+ and Ni for WASP-121b (Hoeijmakers et al. 2020; Borsa et al. 2021; Merritt et al. 2021) using ESPRESSO's high-resolution observations for two transits each. The detection of these species, together with their respective velocities, broadening and depths provide important insights into the composition and dynamics of these extreme atmospheres.

In this study we revisit these datasets and extend the list of currently detected species. This paper is structured as follows. In Section 2, we describe the observations taken and on Section 3 we show how we reduce the data, extract the planetary spectra, and cross-correlate these spectra with synthetic spectra specifically designed for ultra-hot Jupiters. The results and discussion are then given in Section 4.

2. Observational data

In this work we study the two ultra-hot Jupiters, WASP-76b and WASP-121b. For each target we analyse data from two transits observed with ESPRESSO. These same datasets have recently been studied and led to the detection of multiple species for each of the planets (WASP-76b: Tabernero et al. 2021; Kesseli et al. 2022; WASP-121b: Borsa et al. 2021). The 1UT observations used in this work were obtained as part of the ESPRESSO Guaranteed Time Observations (programme 1102.C-0744, PI: F. Pepe) covering a wavelength range from 3800 Å to 7880 Å, while using the HR21 mode[2] achieving a resolution of $R \sim 140\,000$. The 4UT observations were taken during ESPRESSO's commissioning using the MR42 mode[3] ($R \sim 70\,000$). The observations are summarized in Table 1, for more information check Tabernero et al. (2021) and Borsa et al. (2021).

The data we used throughout this work were reduced using the version 2.2.8 of the Reduction Software (DRS) pipeline[4]. From the obtained data products, we make use of the sky-subtracted 1D (orders merged) spectra `S1D_SKYSUB_A`.

3. Planetary transmission spectrum and cross-correlation analysis

3.1. Telluric correction

Before light reaches the VLT mirrors, it crosses Earth's atmospheres leaving its imprints on the observed spectra in the form of terrestrial absorption features. To correct for Earth's absorption lines we use the `Molecfit`[5] pipeline (Smette et al. 2015; Kausch et al. 2015) within the `ExoReflex` environment (Freudling et al. 2013) as in Allart et al. (2017). With this same tool we simultaneously account for the Barycentric Earth Radial Velocity (BERV) on each exposure (Allart et al. 2017). The wavelength regions we have used for the fitting of the terrestrial features are: 6890-6900 Å, 7160-7340 Å and 7590-7770 Å (as in Tabernero et al. 2021). These regions are selected because they are rich in telluric lines and poor in stellar features. We alternatively attempted to optimize these regions, by defining a higher number of smaller regions being very careful to exclude any stellar features. However, both reductions produced similar results[6]. In Appendix B we provide our `Molecfit` input parameters together with an illustrative plot of the *before* and *after* telluric correction around a single line of the sodium doublet (5891.58 Å, Fig. B.1).

3.2. Planetary spectrum extraction

To extract the planetary transmission spectrum, we follow a reasoning similar to the techniques outlined by Redfield et al. (2008) and Wyttenbach et al. (2015), which have been successfully applied and improved in many recent studies using high-resolution transmission spectroscopy (e.g. Yan et al. 2017; Allart et al. 2020; Tabernero et al. 2021; Borsa et al. 2021; Casasayas-Barris et al. 2021; Seidel et al. 2022).

We started by shifting each individual spectrum into the reference frame of the star. By applying Keplerian models we correct for the Doppler shifts arising from the planet's orbital pull. We then created a template of the star without any planetary absorption. For this we combined the out-of-transit exposures into a stellar spectrum with high signal-to-noise ratio called the "master-out". To build this master-out, we first corrected for flux variations across the exposures, as due to different atmospheric conditions (airmass, seeing, ...) the shape of the retrieved continuum changes. We started by selecting the lowest airmass spectrum as the reference, and divided each of the individual spectra by this reference. We then masked the region of the spectrum

* e-mail: Tomas.Silva@astro.up.pt
** e-mail: Olivier.Demangeon@astro.up.pt

[1] For these species there are only tentative detections. During our work we confirm as detections the presence of H in WAPS-76b and Mn in WASP-121b.

[2] High resolution with 2×1 binning (Pepe et al. 2021).

[3] Mid resolution with 4× and a 2× binning in the spatial and dispersion directions.

[4] Available at: http://www.eso.org/sci/software/pipelines/index.html

[5] Available at: https://www.eso.org/sci/software/pipelines/skytools/molecfit

[6] Visually comparison, as illustrated on Fig. B.

Table 1: Summary of the transit observations of WASP-76b and WASP-121b.

Target	Night	Exp. time (s)	N_{obs}	$N_{obs,\ in\text{-}transit}$ [a]	Airmass change[b]	S/N@550nm	Mode
WASP-76b	2018-09-03 (N1)	600	35	16 (20)	1.99 - 1.13 - 1.37	∼101	1-UT HR21
WASP-76b	2018-10-31 (N2)	300	70	30 (37)	1.42 - 1.13 - 2.64	∼79	1-UT HR21
WASP-121b	2018-11-30 (N1)	300	29	17 (20)	1.11 - 1.03 - 1.07	∼151	4-UT MR42
WASP-121b	2019-01-06 (N2)	400	52	17 (23)	1.20 - 1.03 - 1.61	∼47	1-UT HR21

Notes. [a] Number of spectra obtained between the second and third contacts, and under parentheses the number for the first to forth contact duration. [b]Airmass change over the night (starting - minimum - ending).

with low signal-to-noise[7] or strong telluric features[8] and fitted a polynomial function (of degree 3) to the unmasked data. We divided out the trend for each of the individual spectra and combined the corrected out-of-transit spectra with a weighted average to create a preliminary master-out, using the inverse square of flux uncertainties as the weights.

We then performed a similar procedure where we instead divided the individual spectra by the created preliminary master-out. The reason for this extra step is so that later all the individual spectra (in-transit and out-of-transit) are divided by the same out-of-transit template. As a result of this division, a clear "wiggle" pattern becomes visible across the spectra. This is to be expected for the ESPRESSO data as noted by Tabernero et al. (2021) and Borsa et al. (2021). In Appendix C we can see the wiggles across the wavelength range for a single exposure of WASP-121b with the 4UT's. The wiggles amplitude and frequency vary across wavelengths and do not behave as perfect sinusoids. To correct for these wiggles together with residual features from the flux normalization, we fitted each spectrum with splines[9]. We then divided our spectra over the fitted splines. An example of this fitting is illustrated on Fig. C.1.

Finally we shifted these individual spectra according to the planet's orbital velocity and computed the weighted averages of the spectral regions of interest, creating masters of the out-of-transit and in-transit data in both the planet's and stellar's rest frame.

3.3. Cross-correlation analysis

With the planetary transmission spectrum retrieved for each of the exposures, we then performed a cross-correlation analysis with all the templates from `The Mantis Network I`[10] (Kitzmann et al. 2021). These templates allow for the use of individual lines that would otherwise go unnoticed due to the high noise in the retrieved planetary spectrum. By using the cross-correlation function (CCF) approach, these individual lines can be combined into a detectable line profile. For the WASP-76b and WASP-121b line mask, we consider an isothermal atmosphere at 2500 K[11], given both planets equilibrium temperatures (West et al. 2016; Delrez et al. 2016) and in line with the application outlined in Kitzmann et al. (2021). The number of lines used per species in our wavelength range can be found in Appendix D.

We computed the CCFs in the planet's rest frame, with the previously mentioned binary masks, using the `SciPy` cross-correlation tool (Virtanen et al. 2020). For an easier visualization of the absorption signal, we also produced tomography plots and computed the absorption across a 2D cross-correlation grid in the Kp - Planet's velocity plane (hereafter - *Kp plots*), for examples see Fig 1.

In the tomography plots, we can observe the signature of the Rossiter-McLaughlin effect (RM). Given the current limitations and uncertainties (Casasayas-Barris et al. 2021) when modeling the RM and the associated centre to limb variation (CLV), we chose not to attempt to model these effects. Instead of modelling, we masked the region matching the stellar velocities (-15 km/s to +15 km/s in the stellar rest frame) and combined the remaining signal[12]. An illustration of this masking for the F9 mask can be found in Appendix E.

We fitted Gaussian profiles to the CCFs of the species with visible planetary absorption features. We have used the `lmfit` Python package (Newville et al. 2016) to find the best-fit values and respective uncertainties. For hydrogen we did not perform a CCF[13] but instead directly fitted the Hα line on the retrieved planetary spectrum (master-in). However, we do not expect the Ca+ absorption to follow a Gaussian profile. As mentioned in Borsa et al. (2021), the Ca+ H&K lines are significantly blueshifted and have wider and deeper profiles than any other species, which suggest that it extends beyond the Roche Lobe [14]. The authors also noticed slight asymmetries on these line profiles, and point to planetary atmospheric escape as a possible explanation. In our analysis we found similar results and a clear asymmetric profile for the 4UT partial transit. Both the individual H&K lines, and the combined CCF using the "`Mantis`" mask, show an extended blueshifted absorption (see Fig. F.1) beyond an underlying Gaussian profile, hinting at calcium escaping the planet's atmosphere. A detailed modeling of this profile

[7] Regions where the signal-to-noise is significantly below the baseline ($> 5\sigma$), e.g. <3900 Å.

[8] Regions where the telluric correction was inadequate due to low flux from strong telluric absorption e.g. 6850-7700 Å.

[9] We fit the splines over spectral segments of ∼ 200 Å. As a first step we also tried to fit the wiggles on each exposure using varying sinusoids on limited wavelength intervals, however we found better results with the spline method.

[10] We perform the CCF study with templates from the following species: Li, O, Na, Mg, Al, Si, P, S, K, Ca, Ca+, Sc, Sc+, Ti, Ti+, V, V+, Cr, Cr+, Mn, Mn+, Fe, Fe+, Co, Ni, Ni+, Cu, Zn, Ga, Ge, Rb, Sr, Sr+, Y, Y+, Zr, Zr+, Nb, Mo, Ru, Rh, Pd, Cd, In, Sn, Te, Cs, Ba, Ba+, La, La+, Ce, Ce+, Pr, Nd, Nd+, Sm, Sm+, Eu, Eu+, Gd, Gd+, Tb, Tb+, Dy, Dy+, Ho, Ho+, Er, Er+, Tm, Tm+, Yb, Lu, Lu+, Hf, Hf+, W, Re, Os, Ir, Pt, Tl, Pb, Bi, Th, Th+, U and U+. Some other species were available but with no lines in our wavelength region of interest.

[11] For Fe+, given the empty line list at 2500 K, we used the mask corresponding to a temperature of 3000 K.

[12] Besides the masking of the stellar component, this process also removes part of the planetary signal, which at times can cause a diminished SNR.

[13] There are no available `Mantis` masks for hydrogen.

[14] We estimated the effective planet radius at the line center by assuming $R^2_{eff}/R^2_p = (\delta+h)/\delta$, where δ is the transit depth and h the transmitted line amplitude (Chen et al. 2020). For Ca+ in WASP-121b we find effective radii of ∼1.7 R_p (Night 1) and ∼2.1 R_p (Night 2) in agreement with Borsa et al. (2021)

could confirm this hypothesis and allow an estimate of the atmospheric escape rate of calcium.

4. Results and discussions

In Table 2 we list the species for which a visual inspection showed tentative absorption features, together with the best fit values and uncertainties from the Gaussian fit parameters (amplitude, center RV and full width half maximum - FWHM). The CCF line profile and Kp-plots for each of these can be found in Appendix G.

For WASP-76b, we find a new chemical species in the atmosphere of this planet, Ba+, with a strong absorption signal on both of the observing nights. We also confirm the detections made by Tabernero et al. (2021) and Kesseli et al. (2022) of H, Li, Na, Mg, Ca+, V, Cr, Mn and Fe. The strongest K lines lie in a region that we are excluding due to high telluric contamination; therefore, K is not included in our study. We also do not recover the presence of Co, Ni, Sr+ claimed by Kesseli et al. (2022), possibly due to differences in the retrieval process.

Regarding WASP-121b, we confirm the detections of H, Li, Na, Mg, Ca+, V, Cr, Mn, Fe and Fe+ claimed by Borsa et al. (2021) and of Ca and Ni detected by Merritt et al. (2021). The new species we claim to be present in the atmosphere of WASP-121b are Ba+, Co and Sr+. Besides these, we also find tentative evidence of the presence of Ti+, visible when we remove the signal matching the stellar velocities (see Fig. F.2).

Overall, we see a trend where most of the detected species are blueshifted relative to their expected line positions. This trend was also observed in previous studies (e.g. Cauley et al. 2021; Pai Asnodkar et al. 2022) and is expected to be due to the winds across the terminator, moving from the dayside to the nightside of the planet.

Another surprising finding is the detection of Ba+ in both planets, the heaviest element detected to date in exoplanetary atmospheres. Both WASP-76b and WASP-121b represent some of the highest S/N datasets currently available, the presence in both of the studied planets may indicate that this heavy species can be common in the atmospheres of ultra-hot Jupiters. The CCF plots, tomography plots and Kp-plots are shown in Figs. 1 and 2 for both of the planets. Close to the expected planet velocity we see a clear absorption signal, that follows the planet's Kp across the exposures. We can also observe faint absorption signals directly on the planetary spectrum at the position of the strongest lines of the Ba+ CCF mask (Appendix H). Besides, we also note the ionization trend of these alkaline earth metals (Ca+, Sr+ and Ba+). The presence of these heavy ionized species at high altitudes in the atmospheres of ultra hot jupiters may be evidence of unexpected atmospheric dynamics. Describing the mechanisms that would explain the presence of these species in the upper layers of the atmosphere is beyond the scope of this paper. However, we hope that with this discovery we encourage further atmospheric modeling.

As studied in Borsa et al. (2021), we also note the much higher S/N and clearer absorption features for the lower resolution 4UT partial transit (despite the lower resolution: $\sim$ 70 000), a clear demonstration of the potential of the 16m-equivalent mirror or of future high resolution spectrographs for the ELT (e.g. ANDES - Marconi et al. 2021).

Acknowledgements. This work was supported by Fundação para a Ciência e a Tecnologia (FCT) and Fundo Europeu de Desenvolvimento Regional (FEDER) via COMPETE2020 through the research grants UIDB/04434/2020, UIDP/04434/2020, PTDC/FIS-AST/32113/2017 & POCI-01-0145-FEDER-032113, PTDC/FIS-AST/28953/2017 & POCI-01-0145-FEDER-028953. This work has been carried out in the frame of the National Centre for Competence in Research PlanetS supported by the Swiss National Science Foundation (SNSF). This project has received funding from the European Research Council (ERC) under the European Union's Horizon 2020 research and innovation programme (project Spice Dune, grant agreement No 947634). This project has received funding from the European Research Council (ERC) under the European Union's Horizon 2020 research and innovation programme (project Four Aces; grant agreement No 724427). T.A.S acknowledges support from the Fundação para a Ciência e a Tecnologia (FCT) through the Fellowship PD/BD/150416/2019 and POCH/FSE (EC). O.D.S.D. is supported in the form of work contract (DL 57/2016/CP1364/CT0004) funded by FCT. R. A. is a Trottier Postdoctoral Fellow and acknowledges support from the Trottier Family Foundation. This work was supported in part through a grant from FRQNT. This work has been carried out within the framework of the National Centre of Competence in Research PlanetS supported by the Swiss National Science Foundation. The authors acknowledge the financial support of the SNSF. F.B. acknowledges support from PRIN INAF 2019 CJM acknowledges FCT and POCH/FSE (EC) support through Investigador FCT Contract 2021.01214.CEECIND/CP1658/CT0001. H.M.T. acknowledges financial support from the Agencia Estatal de Investigación of the Ministerio de Ciencia, Innovación y Universidades through project PID2019-109522GB-C51/AEI/10.13039/50110001103 E. E-B. acknowledges financial support from the European Union and the State Agency of Investigation of the Spanish Ministry of Science and Innovation (MICINN) under the grant PRE2020-093107 of the Pre-Doc Program for the Training of Doctors (FPI-SO) through FSE funds. F.P.E. and C.L.O. would like to acknowledge the Swiss National Science Foundation (SNSF) for supporting research with ESPRESSO through the SNSF grants nr. 140649, 152721, 166227 and 184618. The ESPRESSO Instrument Project was partially funded through SNSF's FLARE Programme for large infrastructures. Y.A. acknowledges the support of the Swiss National Fund under grant 200020_172746. D.E. acknowledges financial support from the Swiss National Science Foundation for project 200021_200726. N.J.N. was financed by projects POCI-01-0145-FEDER-028987, PTDC/FIS-AST/28987/2017, PTDC/FIS-AST/0054/2021 and EXPL/FIS-AST/1368/2021, as well as UIDB/04434/2020 & UIDP/04434/2020, CERN/FIS-PAR/0037/2019, PTDC/FIS-OUT/29048/2017. A.S.M. acknowledges financial support from the Spanish Ministry of Science and Innovation (MICINN) under 2018 Juan de la Cierva program IJC2018-035229-I. A. S. M. acknowledges financial support from the MICINN project PID2020-117493GB-I00 and from the Government of the Canary Islands project ProID2020010129.

References

Allart, R., Lovis, C., Pino, L., et al. 2017, A&A, 606, A144
Allart, R., Pino, L., Lovis, C., et al. 2020, A&A, 644, A155
Borsa, F., Allart, R., Casasayas-Barris, N., et al. 2021, A&A, 645, A24
Bourrier, V., Ehrenreich, D., Lendl, M., et al. 2020, A&A, 635, A205
Casasayas-Barris, N., Palle, E., Stangret, M., et al. 2021, A&A, 647, A26
Casasayas-Barris, N., Pallé, E., Yan, F., et al. 2019, A&A, 628, A9
Cauley, P. W., Wang, J., Shkolnik, E. L., et al. 2021, AJ, 161, 152
Chen, G., Casasayas-Barris, N., Pallé, E., et al. 2020, A&A, 635, A171
Delrez, L., Santerne, A., Almenara, J. M., et al. 2016, MNRAS, 458, 4025
Ehrenreich, D., Lovis, C., Allart, R., et al. 2020, Nature, 580, 597
Fortney, J. J., Dawson, R. I., & Komacek, T. D. 2021, Journal of Geophysical Research (Planets), 126, e06629
Freudling, W., Romaniello, M., Bramich, D. M., et al. 2013, A&A, 559, A96
Hoeijmakers, H. J., Seidel, J. V., Pino, L., et al. 2020, A&A, 641, A123
Høg, E., Fabricius, C., Makarov, V. V., et al. 2000, A&A, 355, L27
Kausch, W., Noll, S., Smette, A., et al. 2015, A&A, 576, A78
Kesseli, A. Y., Snellen, I. A. G., Casasayas-Barris, N., Mollière, P., & Sánchez-López, A. 2022, AJ, 163, 107
Kitzmann, D., Hoeijmakers, J. H., Grimm, S. L., et al. 2021, arXiv e-prints, arXiv:2112.11380
Marconi, A., Abreu, M., Adibekyan, V., et al. 2021, The Messenger, 182, 27
Merritt, S. R., Gibson, N. P., Nugroho, S. K., et al. 2021, MNRAS, 506, 3853
Newville, M., Stensitzki, T., Allen, D. B., et al. 2016, Lmfit: Non-Linear Least-Square Minimization and Curve-Fitting for Python, Astrophysics Source Code Library, record ascl:1606.014
Pai Asnodkar, A., Wang, J., Eastman, J. D., et al. 2022, AJ, 163, 155
Pepe, F., Cristiani, S., Rebolo, R., et al. 2021, A&A, 645, A96
Pepe, F. A., Cristiani, S., Rebolo Lopez, R., et al. 2010, in Society of Photo-Optical Instrumentation Engineers (SPIE) Conference Series, Vol. 7735, Ground-based and Airborne Instrumentation for Astronomy III, ed. I. S. McLean, S. K. Ramsay, & H. Takami, 77350F
Redfield, S., Endl, M., Cochran, W. D., & Koesterke, L. 2008, ApJ, 673, L87
Sánchez-López, A., Landman, R., Mollière, P., et al. 2022, A&A, 661, A78
Seidel, J. V., Cegla, H. M., Doyle, L., et al. 2022, MNRAS, 513, L15
Seidel, J. V., Ehrenreich, D., Allart, R., et al. 2021, A&A, 653, A73

Seidel, J. V., Ehrenreich, D., Wyttenbach, A., et al. 2019, A&A, 623, A166
Smette, A., Sana, H., Noll, S., et al. 2015, A&A, 576, A77
Tabernero, H. M., Zapatero Osorio, M. R., Allart, R., et al. 2021, A&A, 646, A158
Virtanen, P., Gommers, R., Oliphant, T. E., et al. 2020, Nature Methods, 17, 261
West, R. G., Hellier, C., Almenara, J. M., et al. 2016, A&A, 585, A126
Wyttenbach, A., Ehrenreich, D., Lovis, C., Udry, S., & Pepe, F. 2015, A&A, 577, A62
Yan, F. & Henning, T. 2018, Nature Astronomy, 2, 714
Yan, F., Pallé, E., Fosbury, R. A. E., Petr-Gotzens, M. G., & Henning, T. 2017, A&A, 603, A73

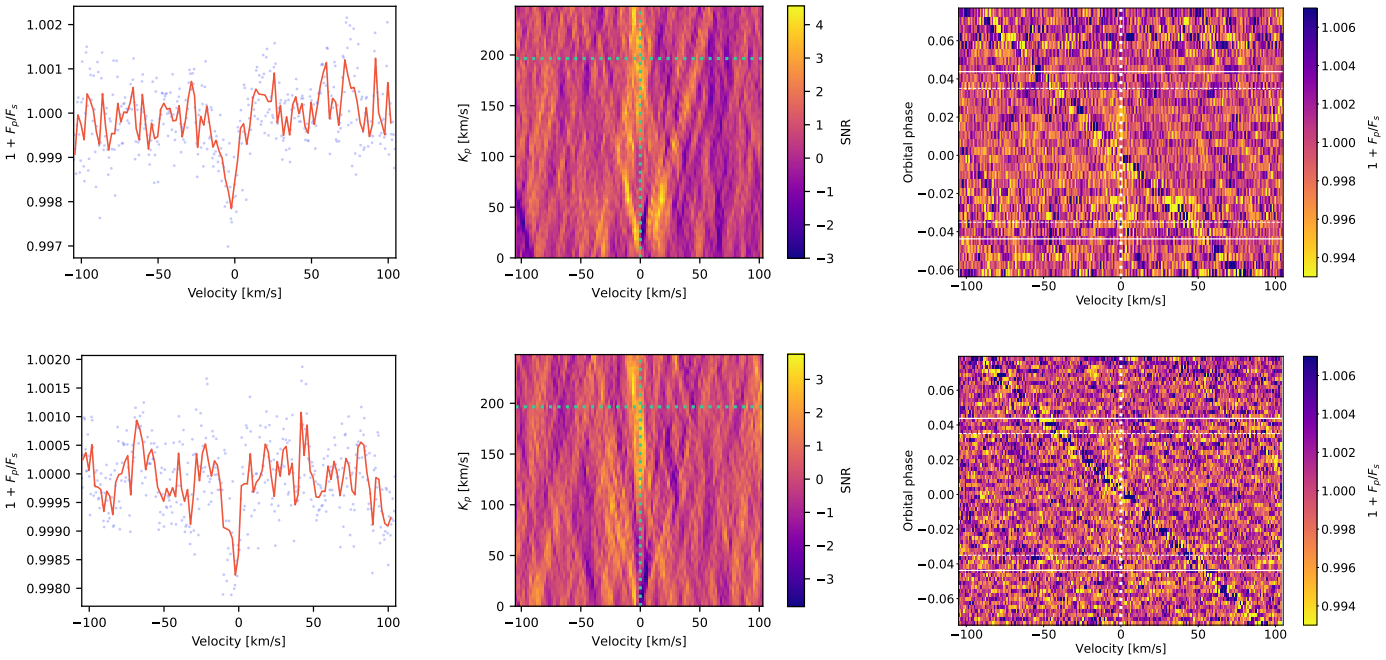

Fig. 1: cross-correlation of the Ba+ mask with the retrieved planetary spectra for both observation nights of WASP-76b (**Top**: 2018-09-03 and **Bottom**: 2018-10-31). **Left:** cross-correlation functions (CCFs) of the averaged in-transit exposures on the planetary frame of reference. **Center:** *Kp-plots* - Map of the sum of all the individual exposures in the planet's rest frame across different values in the *Kp - Planet's velocity* plane. The green dashed lines represent the expected position of the planetary signal on this map. **Right:** Tomographic plots in the planetary rest frame. The white lines represent the transit contacts.

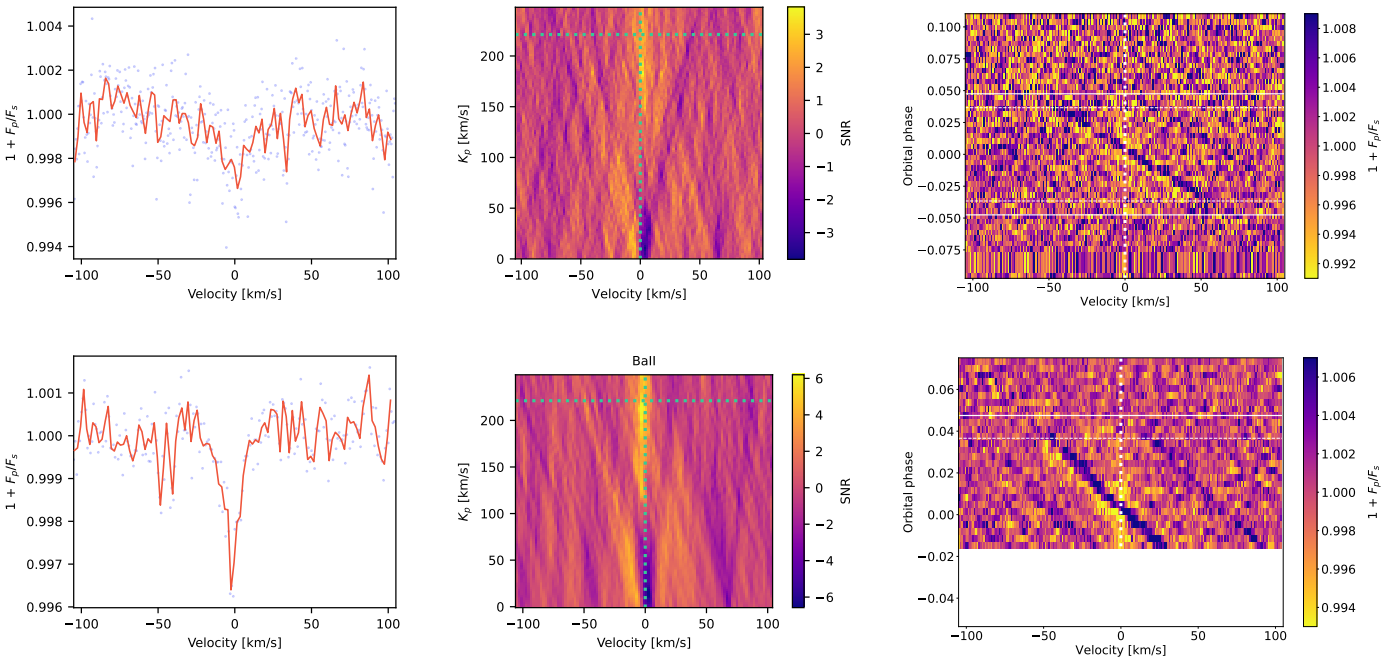

Fig. 2: Same as Fig. 1, but for the WASP-121b observing nights (**Top**: 1UT mode - 2018-11-30; **Bottom**: 4UT mode - 2019-01-06).

Table 2: Summary of the Gaussian fit parameters for the detected species on the transits of WASP-76b and WASP-121b.

		WASP-76				WASP-121			
Species	Night	Amplitude [ppm]	Center RV [km s^{-1}]	FWHM [km s^{-1}]	SNR[c]	Amplitude [ppm]	Center RV [km s^{-1}]	FWHM [km s^{-1}]	SNR[c]
Ba+	N1	1803 ± 205	-3.74 ± 0.74	13.3 ± 1.8	7.0	2270 ± 296	0.5 ± 1.6	30.5 ± 5.8	6.2
	N2	1873 ± 198	-4.0 ± 0.58	10.7 ± 1.1	7.4	2926 ± 258	-1.9 ± 0.5	12.0 ± 1.3	10.6
Ca	N1	-	-	-	-	531 ± 131	0.3 ± 1.4	11.1 ± 2.9	2.6
	N2	-	-	-	-	748 ± 134	-2.13 ± 0.72	8.2 ± 1.7	6.5
Ca+[a]	N1	26517 ± 1846	2.2 ± 1.4	43.1 ± 4.0	26.6	29182 ± 2620	-18.3 ± 3.0	61.1 ± 5.5	28.6
	N2	30870 ± 2527	3.0 ± 0.9	23.7 ± 2.4		54867 ± 900	-10.12 ± 0.72	92.7 ± 1.8	17.2
Co	N1	-	-	-	-	1182 ± 146	1.8 ± 0.6	9.5 ± 1.2	6.3
	N2	-	-	-	-	711 ± 88	-1.11 ± 0.94	16.7 ± 2.7	5.7
Cr	N1	383 ± 51	-5.44 ± 0.67	10.5 ± 1.7	10.0	9648 ± 72	-1.1 ± 1.0	18.3 ± 2.3	6.4
	N2	314 ± 36	-7.1 ± 1.6	30.4 ± 4.9	9.1	449 ± 60	-2.66 ± 0.88	12.2 ± 1.7	10.9
Fe	N1	667 ± 47	-3.42 ± 0.34	9.01 ± 0.68	13.5	1300 ± 72	-0.27 ± 0.32	11.1 ± 0.64	13.7
	N2	724 ± 36	-3.92 ± 0.34	13.88 ± 0.77	22.2	1141 ± 65	-2.6 ± 0.3	10.7 ± 0.68	16.3
Fe+	N1	-	-	-	-	2395 ± 366	1.1 ± 0.8	9.8 ± 1.5	4.8
	N2	-	-	-	-	2021 ± 299	-2.46 ± 0.63	8.5 ± 1.3	8.3
H[b]	N1	1861 ± 319	3.1 ± 4.8	43 ± 10	5.5	11085 ± 698	-2.6 ± 1.0	31.3 ± 2.0	14.8
	N2	1488 ± 373	-3.0 ± 2.7	19.2 ± 4.0	2.4	15692 ± 458	-1.57 ± 0.46	33.5 ± 1.2	46.4
Li	N1	1606 ± 153	-1.4 ± 1.2	27.6 ± 3.0	6.8	1063 ± 437	-2.9 ± 2.6	11.3 ± 4.3	2.1
	N2	1558 ± 157	-2.41 ± 0.92	17.2 ± 1.8	6.4	2163 ± 305	-8.5 ± 1.4	20.6 ± 3.2	5.2
Mg	N1	873 ± 193	-1.3 ± 2.1	17.7 ± 3.7	4.4	2821 ± 579	-2.4 ± 1.4	10.3 ± 2.8	6.2
	N2	2578 ± 237	-3.25 ± 0.57	12.2 ± 1.1	9.5	2293 ± 316	-2.37 ± 0.82	11.4 ± 1.5	6.9
Mn	N1	1307 ± 119	-3.82 ± 0.57	12.4 ± 1.2	5.9	1005 ± 242	-1.4 ± 1.0	8.0 ± 1.9	2.5
	N2	1406 ± 163	-3.94 ± 0.39	7.1 ± 1.0	7.1	1169 ± 135	-2.0 ± 0.8	13.3 ± 1.5	6.0
Na	N1	1015 ± 88	1.59 ± 0.95	20.7 ± 1.9	10.4	1406 ± 184	-0.98 ± 0.97	14.8 ± 2.2	7.8
	N2	884 ± 79	-0.0 ± 1.0	22.5 ± 2.2	8.9	1245 ± 111	-1.44 ± 0.68	15.1 ± 1.4	10.1
Ni	N1	-	-	-	-	1663 ± 522	-1.52 ± 0.24	1.94 ± 0.98	4.2
	N2	-	-	-	-	611 ± 132	-2.9 ± 1.2	11.4 ± 2.5	5.7
Sr+	N1	-	-	-	-	4548 ± 1092	1.1 ± 3.5	24.0 ± 4.4	5.7
	N2	-	-	-	-	7659 ± 781	-0.24 ± 0.85	15.6 ± 1.6	8.2
V	N1	346 ± 32	-4.88 ± 0.48	10.3 ± 1.0	6.2	618 ± 63	1.94 ± 0.65	12.8 ± 1.7	7.7
	N2	360 ± 26	-4.42 ± 0.53	14.4 ± 1.1	10.6	587 ± 41	-2.13 ± 0.44	13.0 ± 1.1	9.9

Notes. [a] The Ca+ signal is highly asymmetric (see Fig. F.1), as such the Gaussian fit may not be accurate. [b] The H signal corresponds to the direct fit of the observed Hα line in the planetary transmitted spectrum, instead of performing a CCF, as is done with remaining species.
[c] The SNR columns correspond to the significance of the detection. This significance was computed as the ratio of the fitted amplitude to the standard deviation of the binned adjacent continuum (with the a binning width equal to the fitted FWHM).

Appendix A: Parameters

Table A.1: Stellar and planetary parameters.

	WASP-76		WASP-121	
Parameter	Value	Source	Value	Source
Stellar Information				
$T_{\rm eff}$ (K)	6329 ± 65	Ehr2020	6586 ± 59	Bou2021
log g (cgs)	4.196 ± 0.106	Ehr2020	4.47 ± 0.08	Bou2021
[Fe/H] (dex)	0.366 ± 0.053	Ehr2020	0.13 ± 0.04	Bou2021
M_* ($M_\odot$)	1.458 ± 0.021	Ehr2020	1.38 ± 0.02	Bou2021
R_* ($R_\odot$)	1.756 ± 0.071	Ehr2020	1.44 ± 0.03	Bou2021
Age (Gyr)	1.816 ± 0.274	Ehr2020	1.03 ± 0.43	Bou2021
V (mag)	9.52 ± 0.03	Tycho-2	10.51 ± 0.04	Tycho-2
K_s (m s^{-1})	116.02 ± 1.35	Ehr2020	0.177 ± 0.008	Bor2020
Planet Information				
Period [days]	$1.80988198 \pm 0.00000064$	Ehr2020	$1.27492504 \pm 0.00000015$	
T_0 [BJD-2400000]	$58080.626165 \pm 0.0004188$	Ehr2020	58119.72074 ± 0.00017	Bor2020
R_p/R_*	0.10852 ± 0.00096	Ehr2020	0.12534 ± 0.00005	Bor2020
a/R_*	4.08 ± 0.06	Ehr2020	3.8131 ± 0.0075	Bor2020
i [°]	89.623 ± 0.034	Ehr2020	88.49 ± 0.16	Bor2020
e	0 (fixed)	Ehr2020	0 (fixed)	Bor2020
M_p (M_{Jup})	0.894 ± 0.014	Ehr2020	1.157 ± 0.070	Bor2020
R_p (R_{Jup})	1.854 ± 0.077	Ehr2020	1.753 ± 0.036	Bor2020
K_p (km s^{-1})	196.52 ± 0.94	Ehr2020	221.15 ± 17.00	Calculated

Notes. Ehr2020 - Ehrenreich et al. (2020) , Bou2021 - Borsa et al. (2021), Tycho-2 - Høg et al. (2000), Bor2020 - Bourrier et al. (2020)

Appendix B: Telluric correction - Input parameters and spectrum comparison

Table B.1: Some of the key input parameters used in `Molecfit`.

Parameter key	Value	Description
`LIST_MOLEC`	H2O, O2	List of molecules to be included in the model.
`WAVE_INCLUDE`	0.6890,0.6900, 0.7160,0.7340, 0.7590,0.7770	Wavelength ranges to be included.
`WLG_TO_MICRON`	0.0001	Multiplicative factor applied to the wavelength to express it in micrometres.
`WAVELENGTH_FRAME`	VAC_RV	Wavelength reference frame.
`FTOL`	1e-8	Relative chi-square convergence criterion.
`XTOL`	1e-8	Relative parameter convergence criterion.
`FIT_CONTINUUM`	1	Flag to enable/disable the polynomial fit of the continuum.
`CONTINUUM_N`	4	Degree of the polynomial continuum fit to use per range.
`FIT_RES_GAUSS`	True	Fit resolution by Gaussian.
`RES_GAUSS`	3.5	Initial value for FWHM of the Gaussian in pixels, at the centre of the spectrum.
`LNFL_LINE_DB`	updated_aer_v_3.6[a]	File name of the line list

Notes. Descriptions taken from the `Molecfit` Pipeline User Manual at https://ftp.eso.org/pub/dfs/pipelines/instruments/molecfit/molecfit-pipeline-manual-4.1.pdf. [a]From private communication with Romain Allart due to duplicated lines in the aer3.6 line list (Allart et al. 2017, 2020).

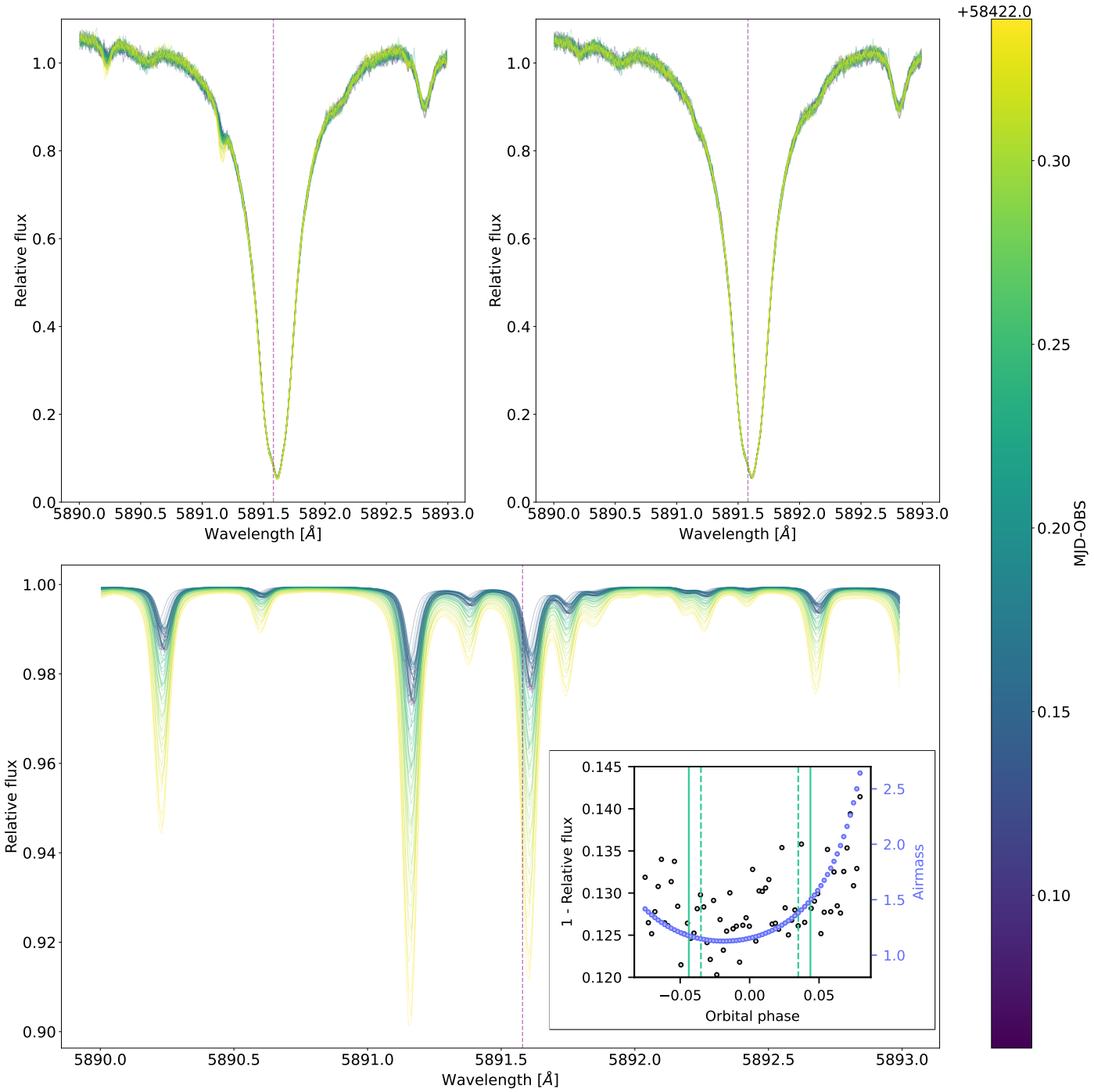

Fig. B.1: Illustration of `Molecfit`'s telluric correction on a single line from the sodium D-lines doublet on the observed spectrum of WASP-76b on the night of 2018-10-31 across exposures. The vertical dashed purple line represents the expected line position. **Top left**: Sodium line prior to the telluric correction. **Top right**: Sodium line after `Molecfit`'s telluric correction. **Bottom**: Ratio of the non-telluric corrected over telluric corrected spectral lines. **Inset**: Flux and airmass variation over the transit observation. As expected for observations later in the night, with higher airmass, the telluric features removed are stronger.

Appendix C: Wiggles

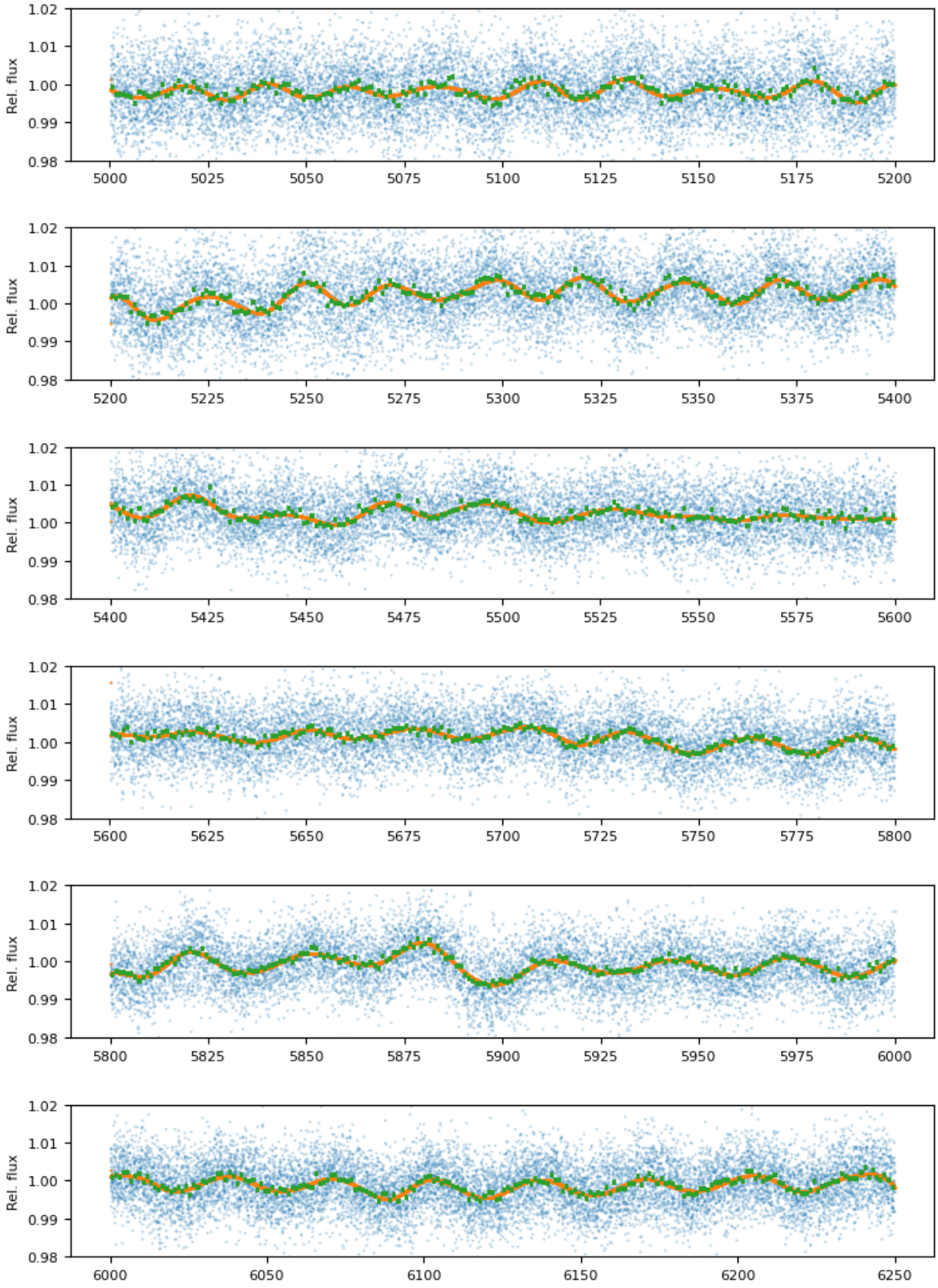

Fig. C.1: (Figure continues on the next page.)

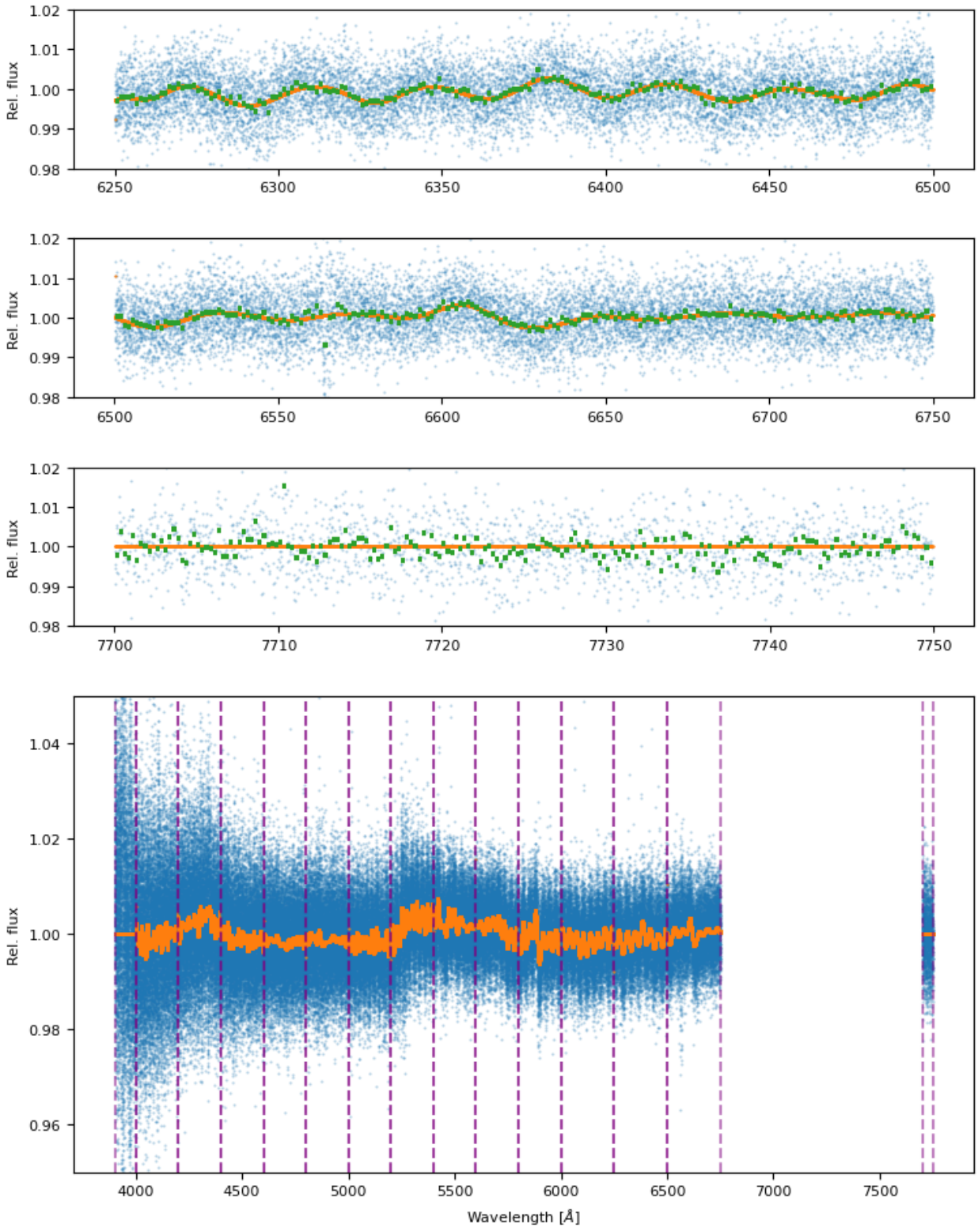

Fig. C.1: Fitting procedure during the wiggle correction step for some of the wavelength regions on the first exposure of the 4UT's observing night of WASP-121b. The fit of the entire spectral range is shown on the last panel. We divide the spectrum into regions (vertical purple lines) where we define the priors and bounds of the fitting functions. For some regions, near the lowest and highest wavelengths, we do not apply the spline fitting, as it would not be a correct match to the observed data.

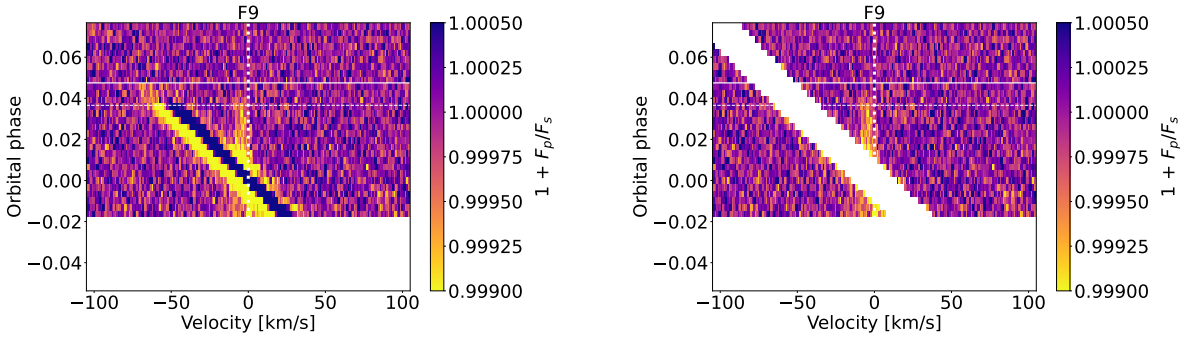

Fig. E.1: Tomography plots in the planetary rest frame built from the WASP-121b CCFs (Night 2 - 4UT's) of the planetary spectrum with the F9 ESPRESSO mask. **Left**: Without masking the stellar signal. **Right**: By masking the stellar velocities ranging from -15 km/s to +15 km/s in the stellar rest frame. The white horizontal band for the early orbital phases originates from the lack of data at the start of transit.

Appendix D: Lines per species used from the `Mantis` masks.

Table D.1: Number of lines per species we have used for our CCFs using the `Mantis` masks at a temperature of 2500 K.

Chemical species	Number of lines
Li	9
Na	43
Mg	52
K	58
Ca	486
Ca+	2
Ti+	9
V	2543
Cr	2096
Mn	362
Fe	3827
Fe+	74[(a)]
Co	984
Ni	580
Sr+	5
Ba+	12

Notes. [a] Lines for the 3000 K template, since there were no lines available at 2500 K.

Appendix E: Stellar signal masking

Appendix F: Calcium II and Titanium II CCFs

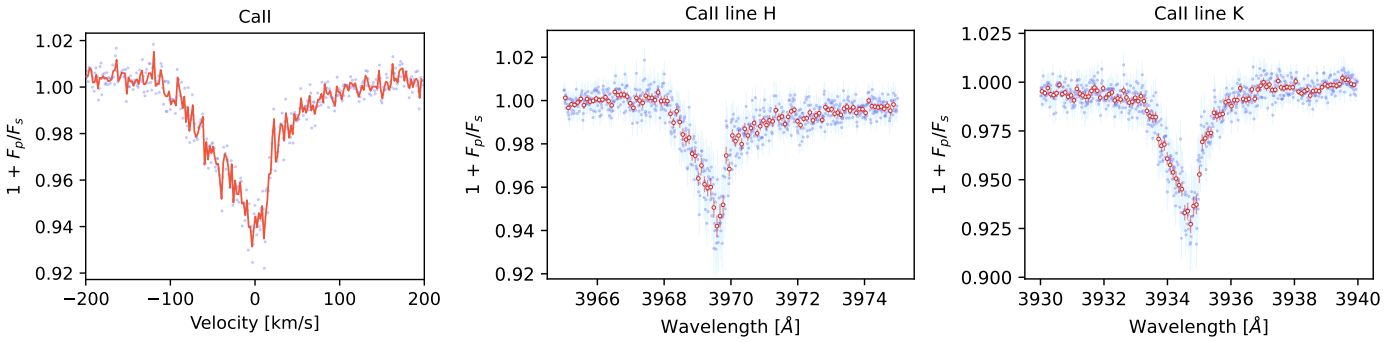

Fig. F.1: **Left**: CCF of the Ca+ mask with the retrieved planetary spectrum for WASP-121b (Night 2 - 4UT's) at the planetary rest frame. **Center and Right**: WASP-121b retrieved planetary spectrum at the Ca+ H&K lines.

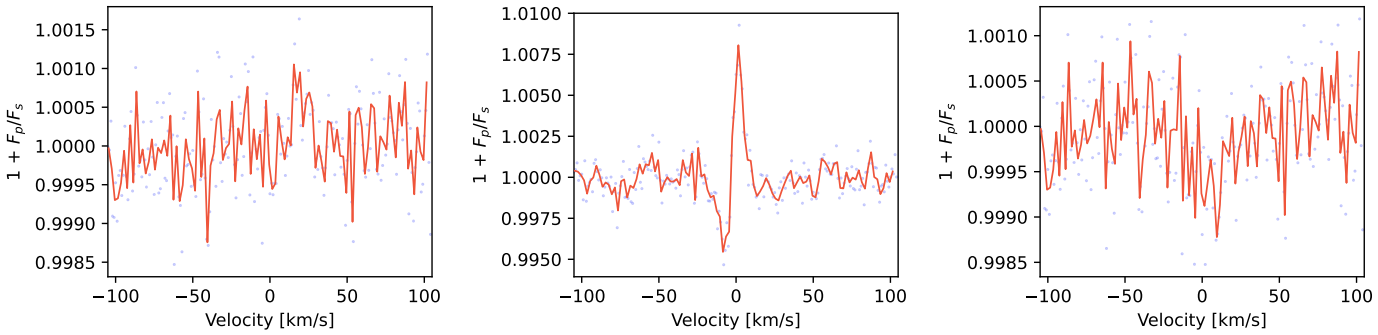

Fig. F.2: **Left**: CCF of the Ti+ mask with the retrieved planetary spectrum for WASP-121b (Night 2 - 4UT's). **Center:** CCF built from only considering the contributions from spectra between -15 km/s and 15 km/s in the stellar frame of reference. **Right**: Same as the initial CCF but excluding the previous stellar contribution region. All the plots are in the planetary rest frame.

Appendix G: CCF & Kp-plots for WASP-76b and WASP-121b

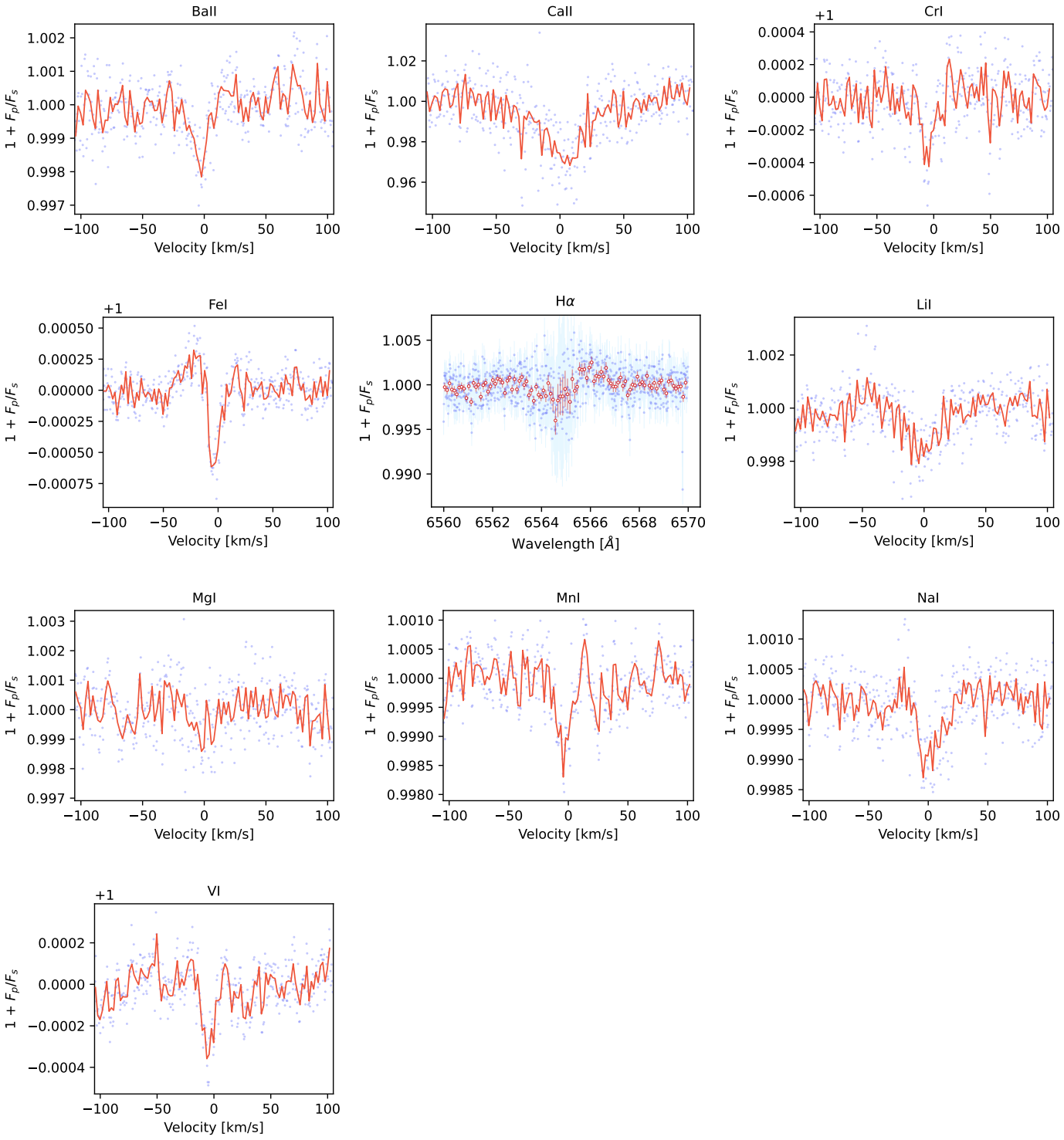

Fig. G.1: WASP-76b - Night 1 (2018-09-03). CCFs of the averaged in-transit exposures on the planetary frame of reference for the detected chemical species. Except for the Hα line, which is present directly in the retrieved planetary spectrum.

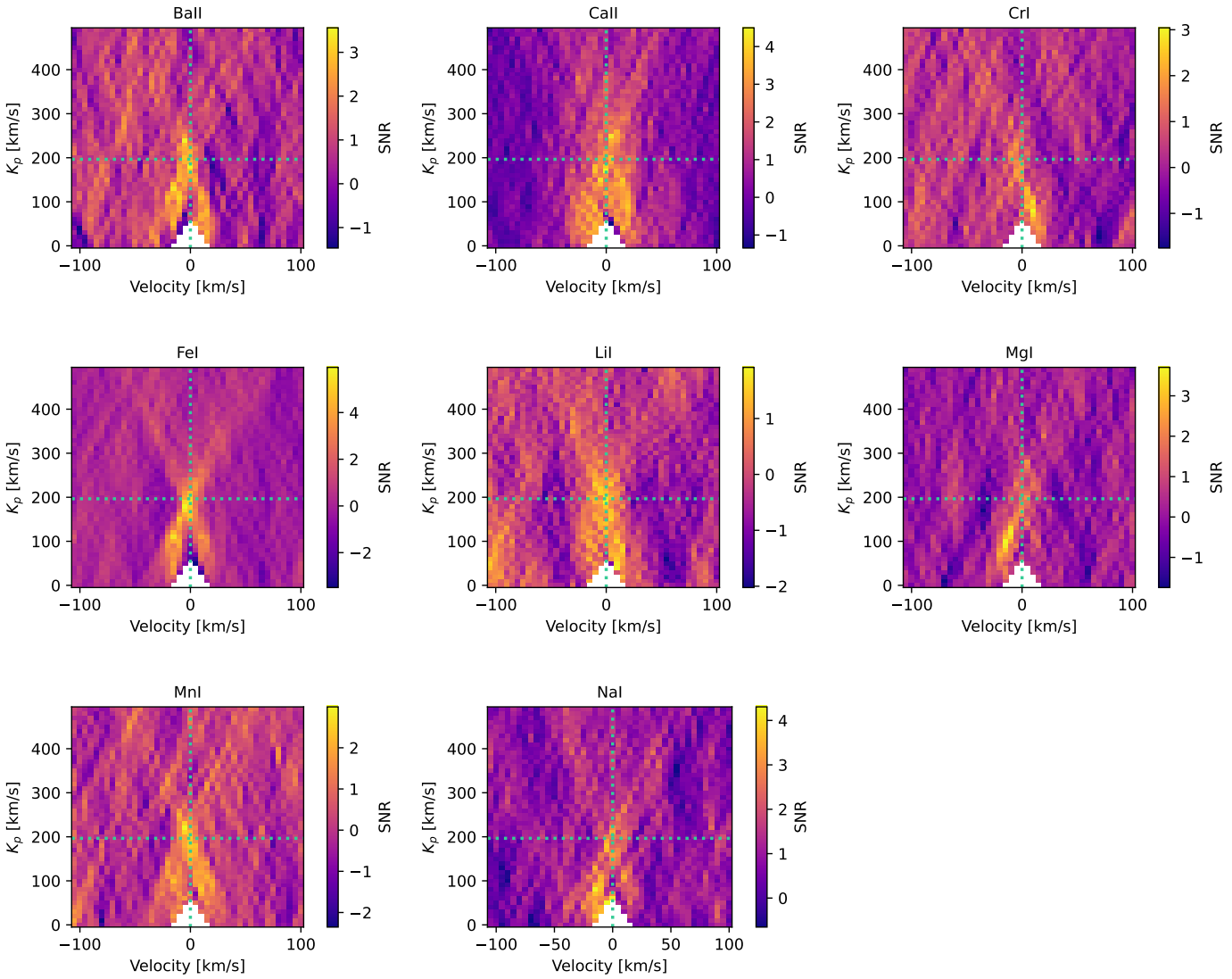

Fig. G.2: WASP-76b - Night 1 (2018-09-03). *Kp-plots* - Map of the sum of all the individual exposures in the planet's rest frame across different values in the *Kp - Planet's velocity* plane. We mask the signal matching the stellar velocities ranging from -15 km/s to +15 km/s in the stellar rest frame. The green dashed lines represent the expected position of the planetary signal on this map.

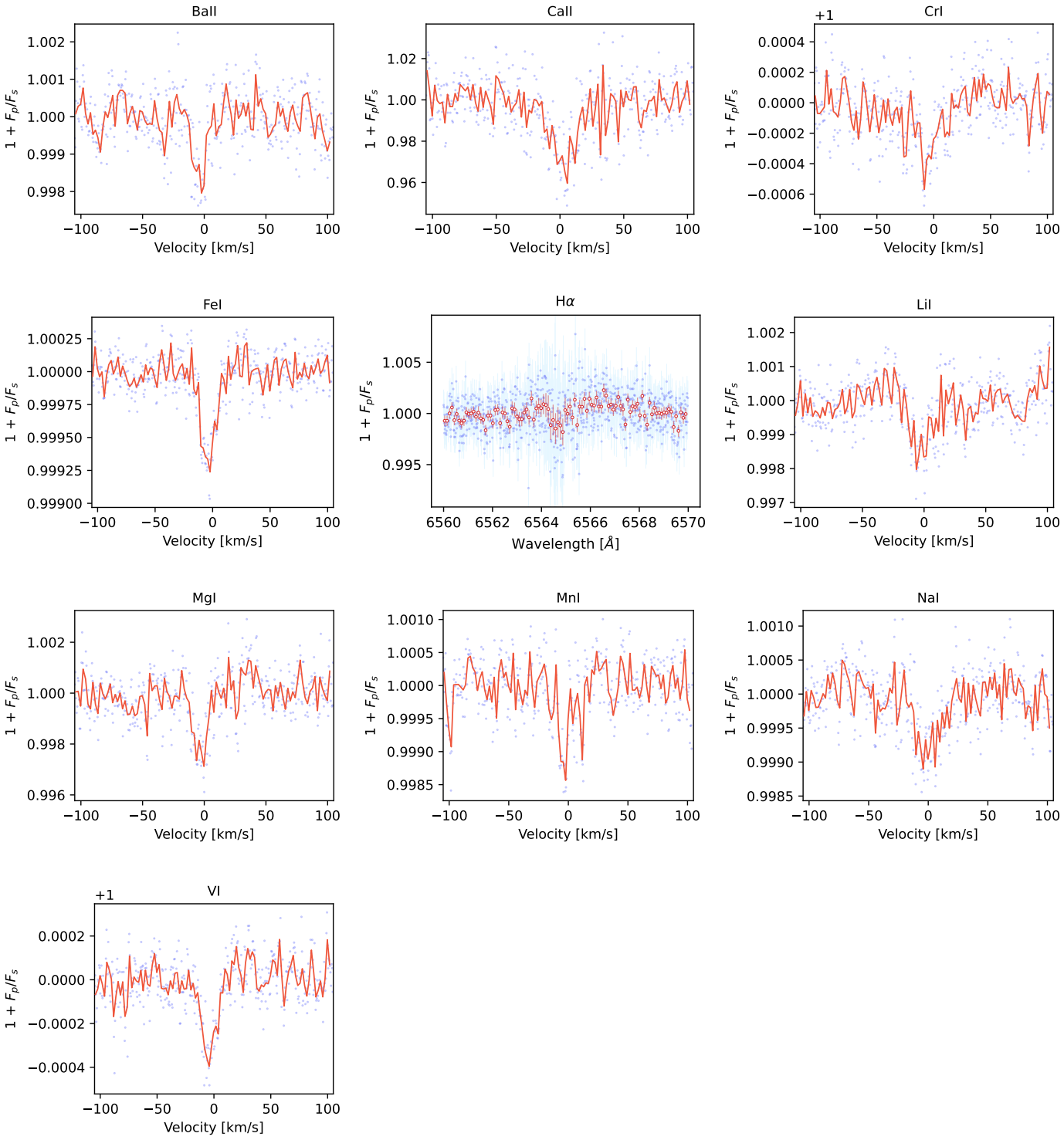

Fig. G.3: Same as Fig. G.1 for WASP-76b Night 2 (2018-10-31).

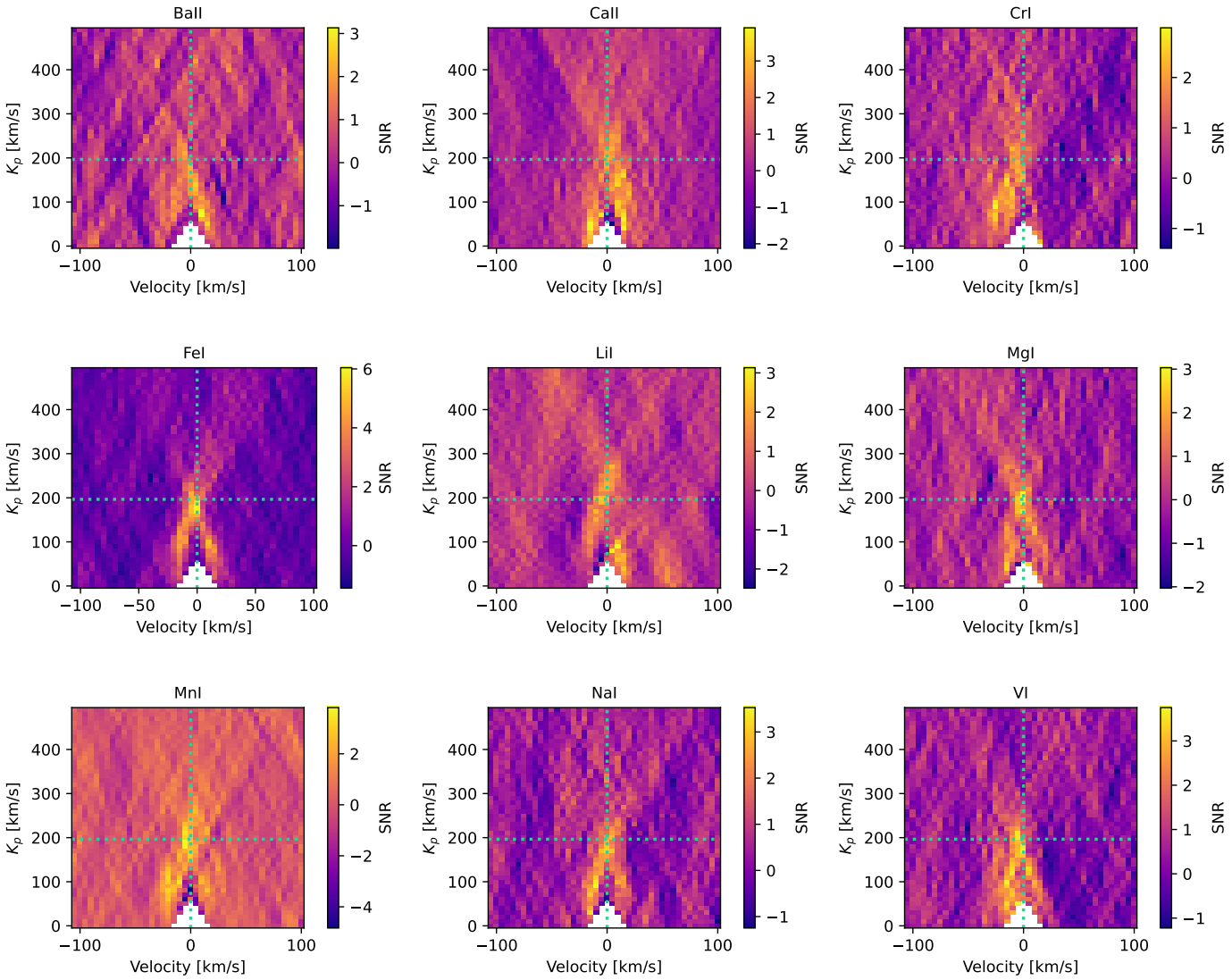

Fig. G.4: Same as Fig. G.2 for WASP-76b Night 2 (2018-10-31).

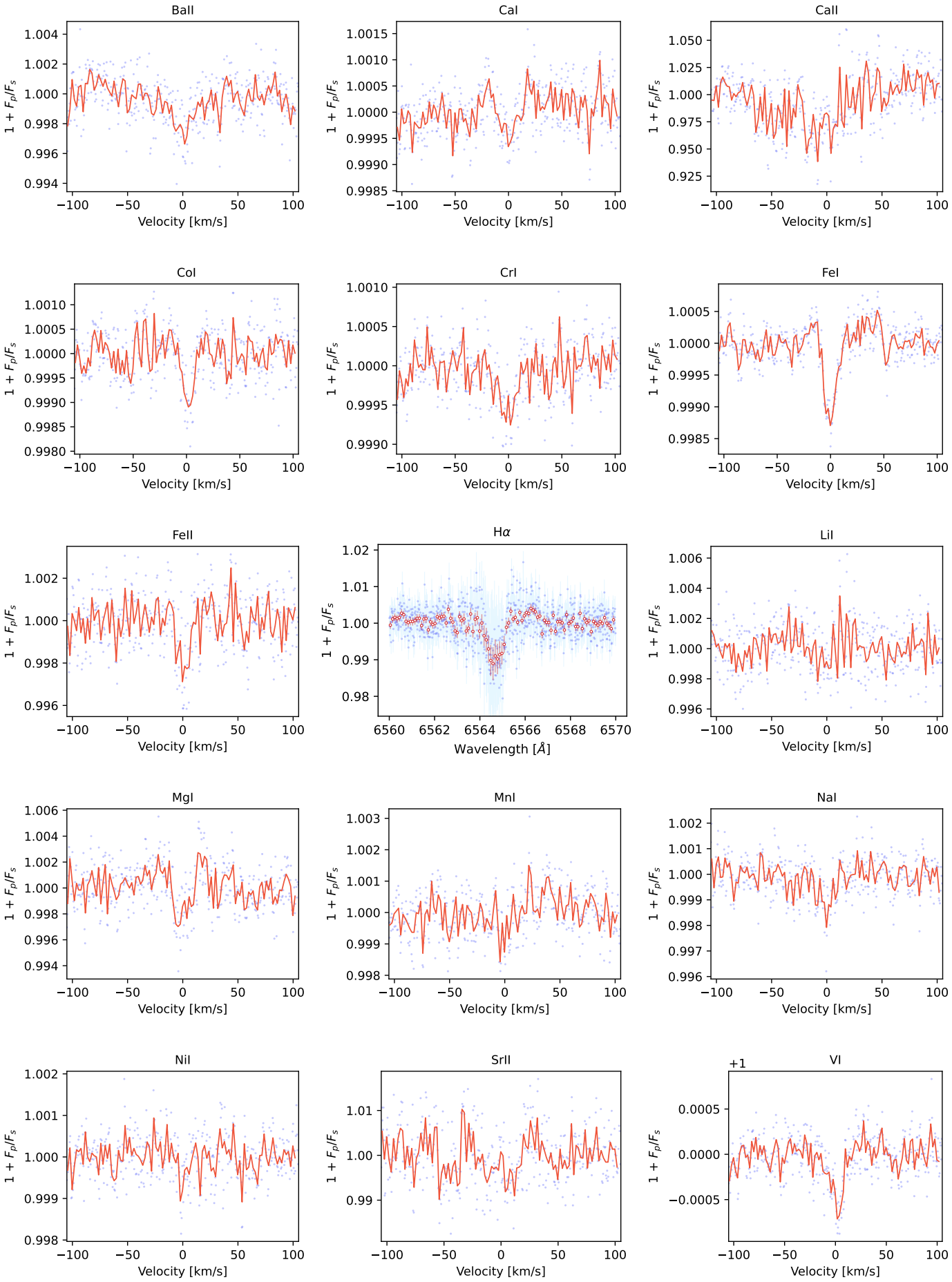

Fig. G.5: Same as Fig. G.1 for WASP-121b Night 1 (1UT - 2018-11-30).

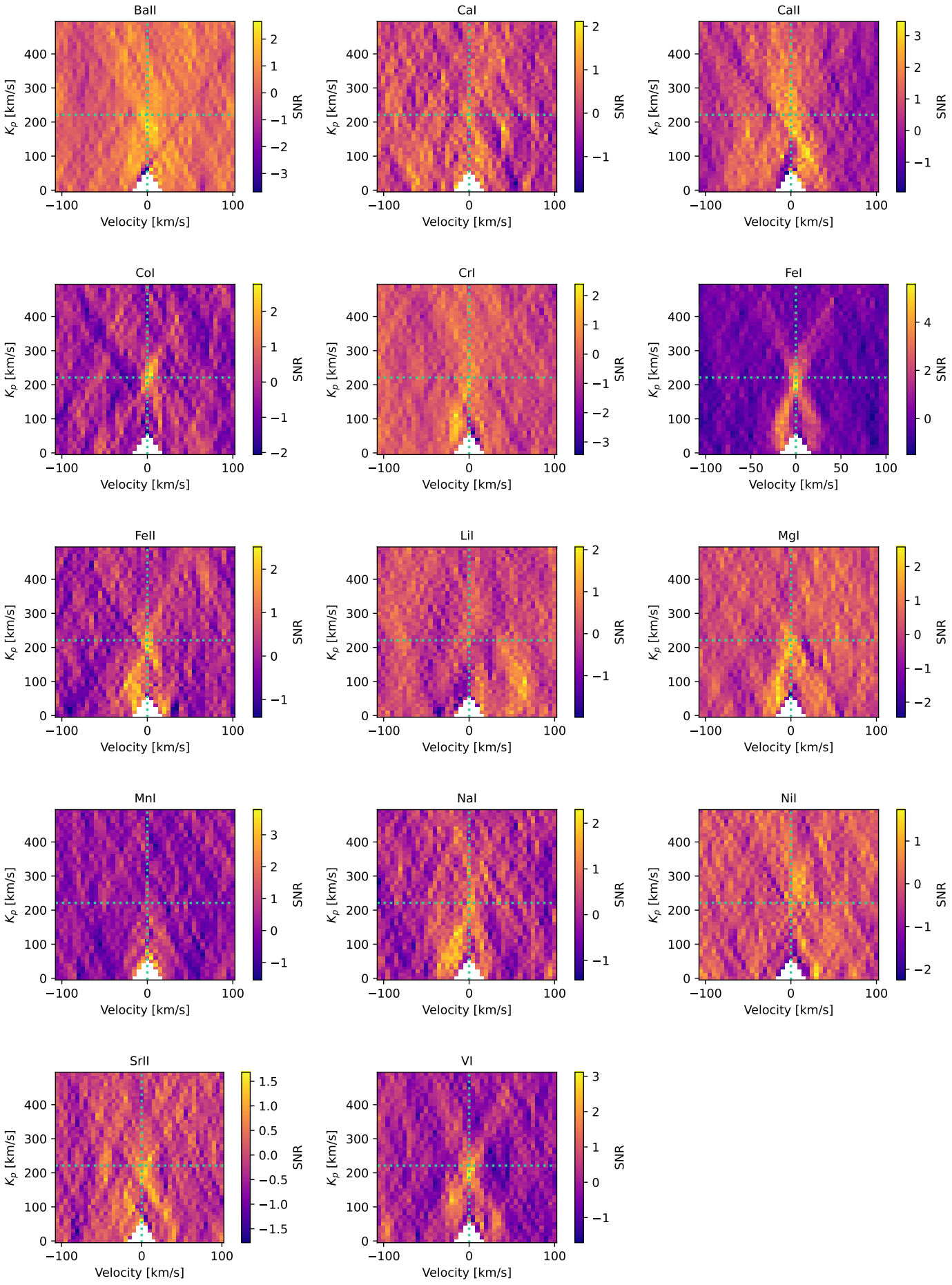

Fig. G.6: Same as Fig. G.2 for WASP-121b Night 1 (1UT - 2018-11-30).

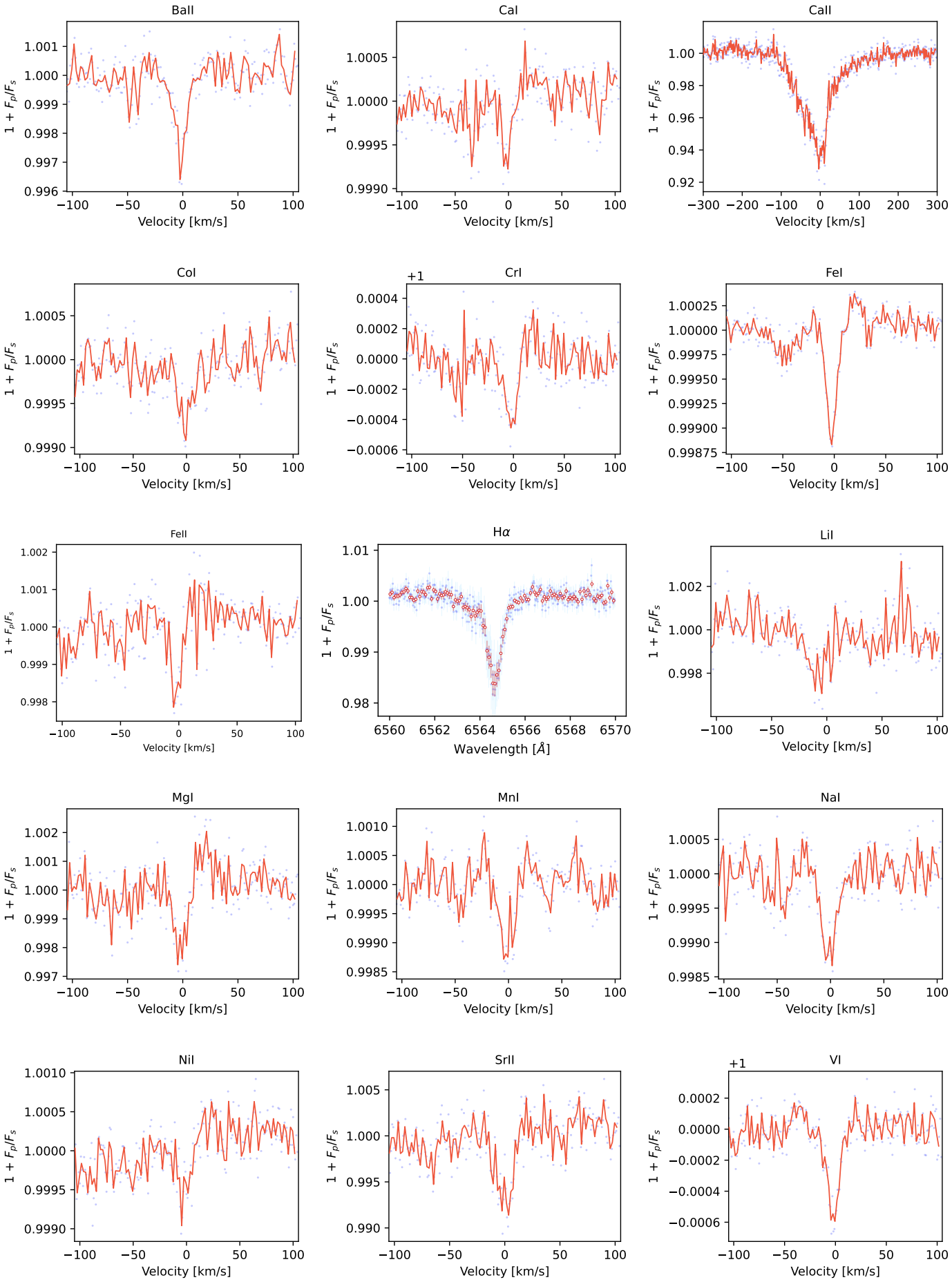

Fig. G.7: Same as Fig. G.1 for WASP-121b Night 2 (4UT's - 2019-01-06).

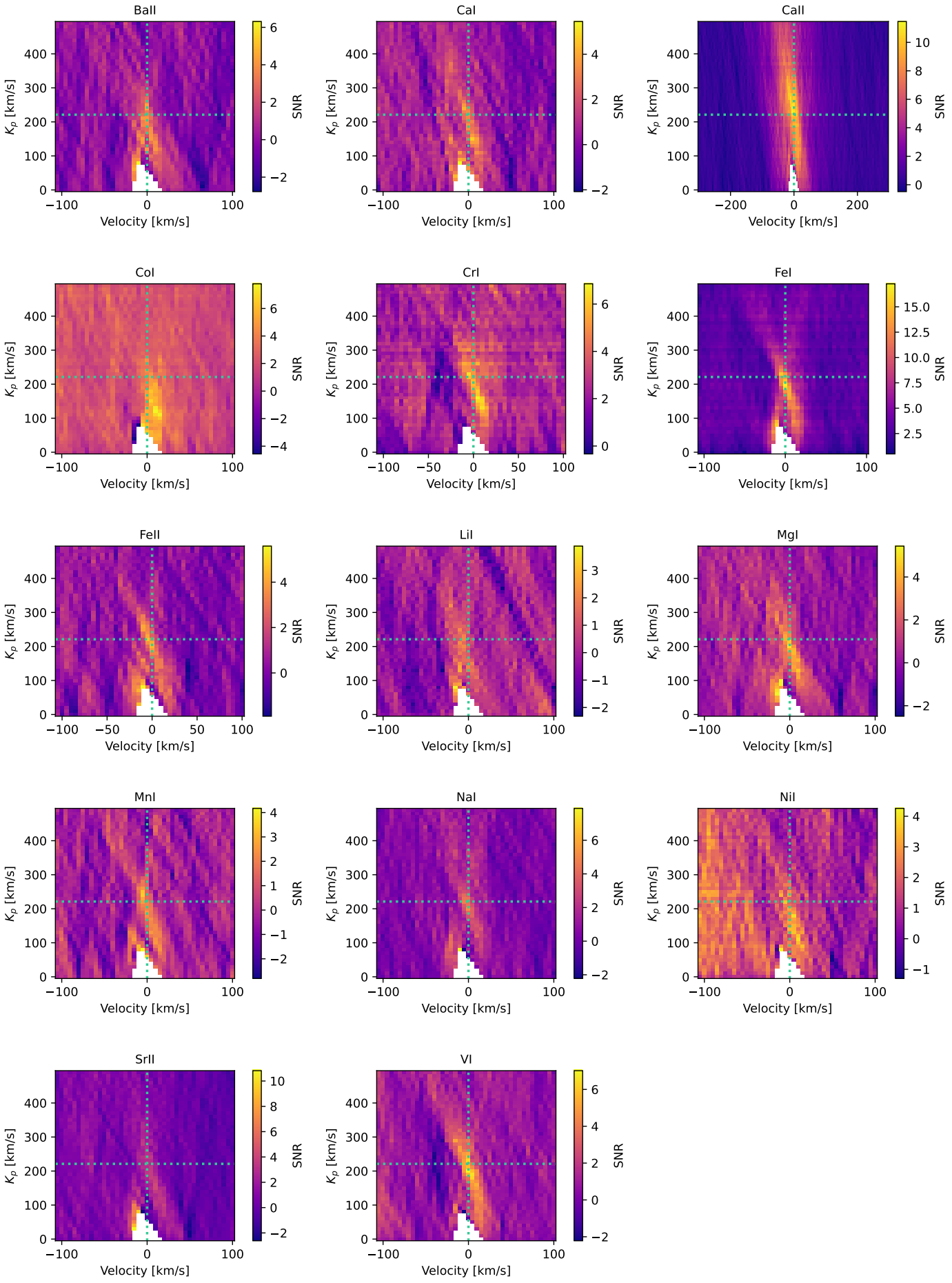

Fig. G.8: Same as Fig. G.2 for WASP-121b Night 2 (4UT's - 2019-01-06)

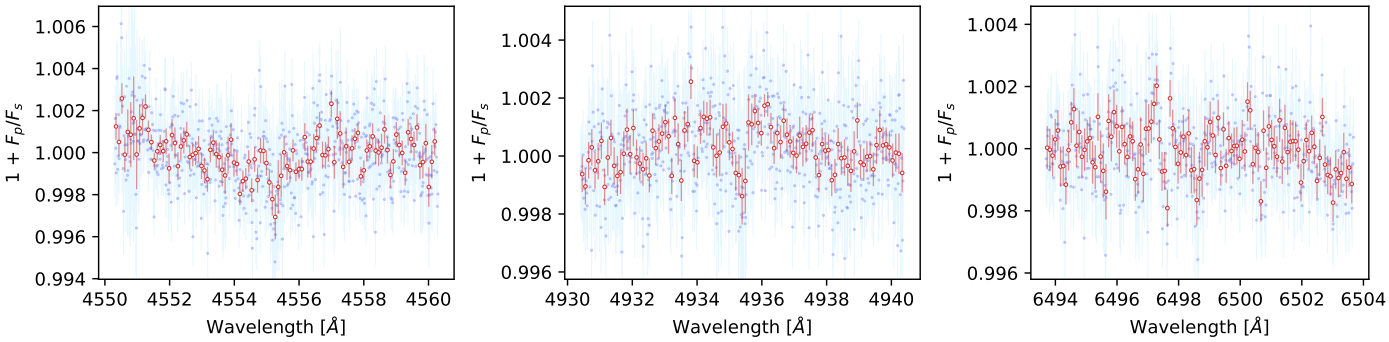

Fig. H.1: Planetary transmission spectrum for the WASP-121b - Night 2 (4UT's - 2019-01-06) dataset, centered at the 3 strongest lines in the barium mask.

Appendix H: Individual Barium II lines